Journal of Experimental and Theoretical Physics, Vol. 101, No. 5, 2005, pp. 770–778.
Translated from Zhurnal Éksperimental'noĭ i Teoreticheskoĭ Fiziki, Vol. 128, No. 5, 2005, pp. 893–903.

ATOMS, MOLECULES, OPTICS

Possibilities of Controlling an X-ray Beam with a Crystal Subjected to Long-Wave Ultrasonic Vibrations

A. E. Blagov[a], M. V. Koval'chuk[a,b], V. G. Kohn[b], V. V. Lider[a], and Yu. V. Pisarevskiĭ[a]

[a]*Shubnikov Institute of Crystallography, Russian Academy of Sciences, Leninskii pr. 59, Moscow, 117333 Russia*
e-mail: aopt@ns.crys.ras.ru
[b]*Kurchatov Institute Russian Research Center, pl. Kurchatova 1, Moscow, 123182 Russia*
Received June 18, 2005

Abstract—X-ray diffraction is experimentally studied in the Laue geometry in a germanium crystal carrying a long-wave ultrasonic wave that creates an alternating lattice deformation along the sample surface. Stroboscopic equipment is used to separate different phases and, correspondingly, different profiles of a spatial deformation distribution from the periodic deformation. A uniform deformation is shown to change the angular position of the X-ray beam, and a nonuniform deformation broadens the angular region of reflection and decreases the peak intensity. Ultrasound can be used to compensate for the static deformation at the place where the single-crystal sample and the resonator are glued together. Apart from the fundamental long-wave harmonic, the crystal contains a parasitic deformation with a shorter wavelength. A simple theoretical model is developed, and it rather accurately describes the experimental results. © *2005 Pleiades Publishing, Inc.*

1. INTRODUCTION

X-ray diffraction in crystals subjected to elastic deformation is now an actively developing field in the solid state physics.

In many works dealing with X-ray-acoustic interactions, researchers aimed to obtain information on the structure of elastic vibrations using X-ray diffraction. This information is important for physical acoustics; moreover, it is widely used to determine the parameters and quality of various piezoelectric and acoustoelectric devices. Some works deal with studying the fundamental features of X-ray-acoustic interaction, such as an X-ray-acoustic resonance [1] resulting in the suppression of the Borrmann effect with ultrasound of a certain frequency.

The possibility of controlling the parameters of an X-ray beam with ultrasound is also of interest; however, the physical foundations of this control depend substantially on the elastic-strain wavelength. We can distinguish two main groups of interaction for different relations between the elastic-strain wavelength Λ and the crystal surface region illuminated by an X-ray beam D.

(1) High frequencies, where $D \gg \Lambda$. In this range, an elastic wave forms a superlattice with a period equal to the ultrasound wavelength. This superlattice results in the formation of additional X-ray diffraction maxima—satellites. This range is studied in most works dealing with X-ray acoustics (e.g., see [2–6] and references therein).

(2) Low and medium frequencies, where $\Lambda \gg D$. This range features an aperiodic (uniform or gradient) lattice deformation across the section (aperture) of the X-ray beam, and this range is poorly understood.

At present, works on controlling the X-ray beam amplitude with ultrasound are advanced. A large set of works dealt with the modulation of an X-ray beam by ultrasound [2–5]. In essence, the authors of these works propose electronic analogs of a mechanical interrupter—chopper [6]. Work [7] on modulation by long-wave ultrasound is also of interest.

Ultrasound can also be used to change the angular position of the diffracted X-ray beam. In the case of low frequencies, this control can be reached by a uniform change in the lattice parameter across the X-ray beam aperture due to the mechanical deformation of an ultrasonic wave in the crystal. Long-wave ultrasound can also create a gradient elastic deformation, which affects the structure of the X-ray beam, in the crystal.

Controlling the spatial position and structure of the X-ray beam with long-wave ultrasound has only been studied in theoretical works [8, 9]. The authors of these works showed that fresh opportunities for developing controlled X-ray optics appear in the case of low-frequency bending ultrasonic vibrations for Bragg diffraction.

In this work, we theoretically and experimentally study the effect of long-wave ultrasonic vibrations on the characteristics of an X-ray beam under conditions of dynamical diffraction. We think that our results can serve as a basis for long-wave ultrasonic vibrations to be applied to control the angular position and spatial structure of the X-ray beam.

1063-7761/05/10105-0770$26.00

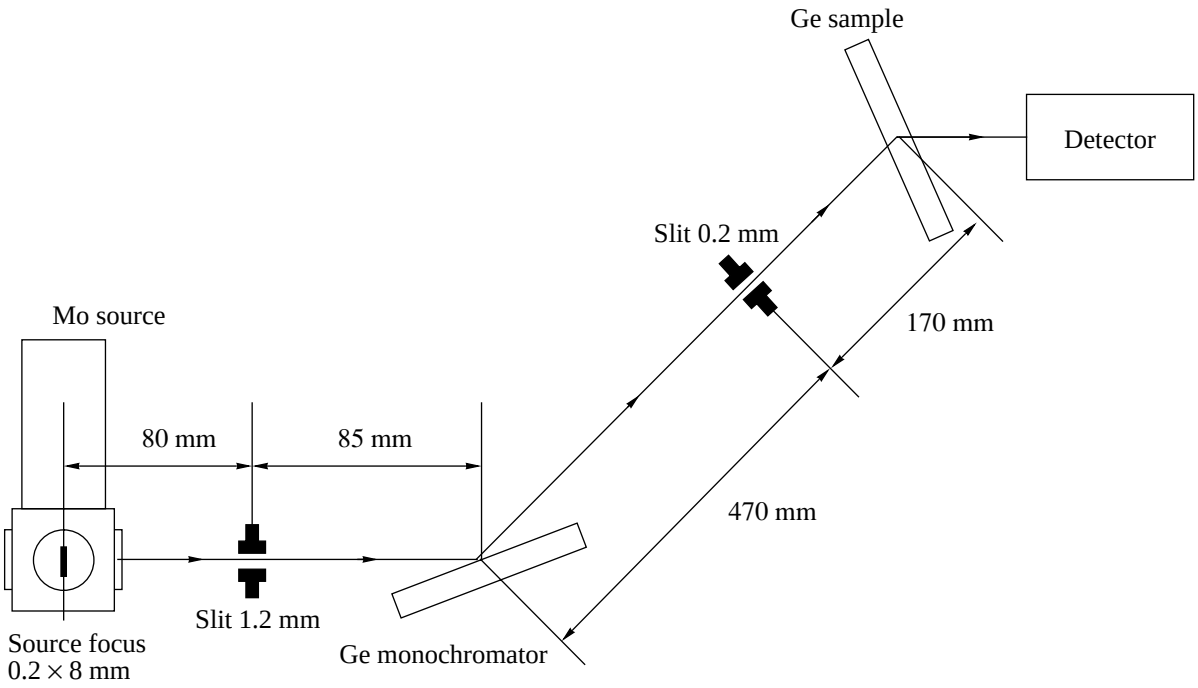

Fig. 1. X-ray optical schematic diagram of the experimental setup.

By analyzing the use of bending vibrations in the Bragg geometry, we revealed substantial difficulties in practical realization of this scheme. Therefore, we designed and actualized a scheme using long-wave ultrasonic vibrations for Laue diffraction. In this work, we present the results of the first stage, where we experimentally confirm and theoretically ground the possibility of controlling the spatial characteristics of the X-ray beam using diffraction in a crystal subjected to long-wave ultrasonic vibrations. In the next section, we describe a designed experimental scheme. In Section 3, we present the time-integrated and stroboscopic experimental results. In Section 4, we develop a theoretical model to analyze the results obtained and show that this model can adequately describe the structure of the appearing deformation from the angular dependence of the intensity of the diffracted X-ray beam.

2. EXPERIMENTAL SCHEME

The experimental setup was based on a TRS-1 X-ray spectrometer [10]. The X-ray optical scheme of the experiment is shown in Fig. 1. We used a double-crystal dispersion-free X-ray diffraction scheme, Mo$K_{\alpha 1}$ radiation, and a 0.2×8-mm^2 radiation-source focus. The angle of the main goniometer was set to an accuracy of $0.025''$. After a crystal monochromator, the collimated beam passes through a 0.2-mm slit in the diffraction plane and falls on the crystal to be studied and subjected to periodic ultrasonic vibrations. The intensity of the diffracted X-ray beam is measured by a BDS scintillation detector.

As the monochromator and samples, we used single-crystal [$1\bar{1}0$] and [111] germanium plates, respectively. In both cases, we generate the symmetrical (220) reflection: the monochromator was in the Bragg diffraction position, whereas the sample was in the Laue diffraction position.

2.1. Scheme for the Excitation of Ultrasonic Vibrations

We used the resonance vibrations of an elastic longitudinal wave along the sample in the Laue diffraction geometry. When vibrations are excited in the crystal, a standing wave with the spatial deformation-amplitude distribution shown in Fig. 2a forms in the ideal case (pure mode). The deformation distribution along the crystal is seen to have the shape of a half-sinusoid with nodes at the sample ends and an antinode at its center. At the center of the crystal, the deformation distribution is quasi-uniform; at its periphery, a near-linear deformation gradient appears, just as a deformation is created in statically bent gradient X-ray monochromators. The difference from this static case consists in a periodic change in the deformation in time.

The samples were $19.5 \times 10 \times 0.4$ mm^3 in size, and their working surface was elongated in the [$1\bar{1}0$] axis. They were part of a composite resonator consisting of a sample and a piezoelectric crystal resonator glued together (Fig. 3). An alternating electromagnetic signal was applied to the lateral faces of the crystal resonator to create longitudinal elastic vibrations along the crys-

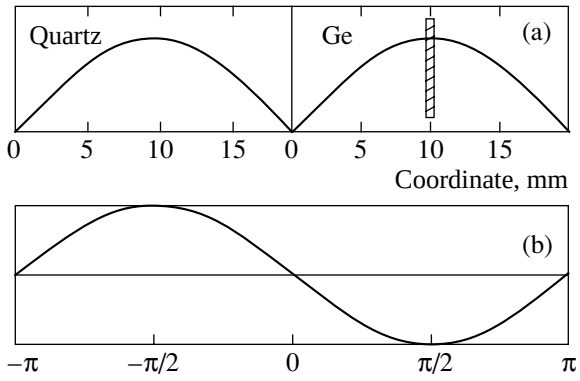

Fig. 2. (a) Estimated spatial distribution of the deformation amplitude in the resonator and sample and (b) the time variation of the deformation. The hatched region demonstrates the area illuminated by the beam of the vibrating crystal.

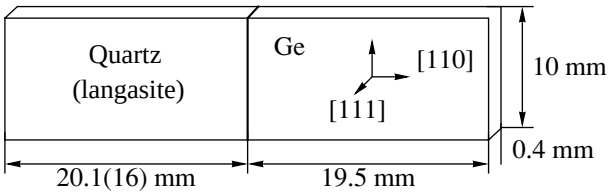

Fig. 3. Schematic diagram of the composite resonator.

tal. To this end, a conducting platinum or nickel layer was deposited on the lateral surfaces by cathode sputtering.

The piezoelectric resonators were made of crystalline quartz with the (XYtwl-18.5°/0°/0°) cut or langasite with the (XYtwl-0°/0°/0°) cut. Such resonators are the best to provide longitudinal tension–compression vibrations almost without parasitic excitation of other vibration types. For effective ultrasound excitation, the resonance frequencies of the sample and the exciting piezoelectric plate must be coincident. In this case, when an alternating electromagnetic signal with a frequency equal to the resonance frequency is applied, high-Q vibrations appear in the crystal–piezoelectric element system. Then, an elastic half-wavelength with a deformation maximum at the center of the crystal is along the length of each plate (Fig. 2a). If parasitic vibrations are not excited, the deformation amplitude is a simple sinusoidal function in space and time (see Fig. 2b). The interface contains a deformation node; therefore, we can retain the high-Q state of the resonance system and rather simply generate high vibration amplitudes.

The resonance frequency of the germanium plate was 126 kHz. The sizes of the piezoelectric elements were chosen so that the resonance frequencies were equal, since vibration excitation was most effective in this case. To generate a pure vibration mode, the width of the piezoelectric element was several times smaller than its length. Using this experimental scheme, we can measure a diffraction reflection curve (DRC) averaged over the ultrasound period, i.e., the angular dependence of the intensity of the diffracted X-ray beam for a small rotation of the sample about the X-ray beam.

2.2. Reflected-Beam Detecting Unit

The unit for detecting the intensity of the diffracted X-ray beam consisted of a scintillation detector of X-ray quanta, an amplifier with a discriminator, and a stroboscopic system (Fig. 4). This scheme allowed us to count X-ray quanta reflected by the crystal under study both continuously and periodically. The counting system processed and converted signals from the detector, and the stroboscopic system differentiated them with respect to time (i.e., presented them as a function of the crystal vibration phase).

In the stroboscopic experiments, a synchronizing signal from the sinusoidal-signal generator that excited the crystal resonator was applied to a pulse generator, whose main purpose was to form a pulse displaced in phase with respect to the synchronizing signal. The pulse generator generated pulses having the crystal-resonator vibration frequency and a controlled phase shift with respect to crystal-resonator vibrations (the vibration phase was set to an accuracy of 10%). According to each coming pulse, the coincidence circuit allowed the counting system to count the X-ray quanta reflected by the sample. The counting time (the time of recording signals from the detector) was set in the coincidence circuit and was one-tenth of the resonator vibration period. Using this scheme, we could detect the diffracted X-ray beam only at a given resonator vibration phase.

3. EXPERIMENTAL RESULTS

We experimentally studied X-ray-acoustic interaction during the excitation of long-wave ultrasound with and without stroboscopic analysis. As noted above, in the absence of excited parasitic vibrations, the deformation amplitude should be a simple sinusoidal function in space and time. If the crystal length is much larger than the X-ray beam width, we can change the distribution (gradient) of the ultrasonic-deformation amplitude within the X-ray beam width by moving the crystal with respect to the X-ray beam.

3.1. Time-Integrated Measurements

The evolution of DRC measured when the position of the X-ray beam is scanned from the free end of the sample to the place of gluing with the piezoelectric transducer without stroboscopy gives information on an actual deformation distribution along the crystal. The sample thickness meets the conditions of the Borrmann effect with an absorption factor $\mu t \approx 12$ (where μ is the linear absorption factor and t is the sample thickness). The samples, i.e., the germanium plates, have a high

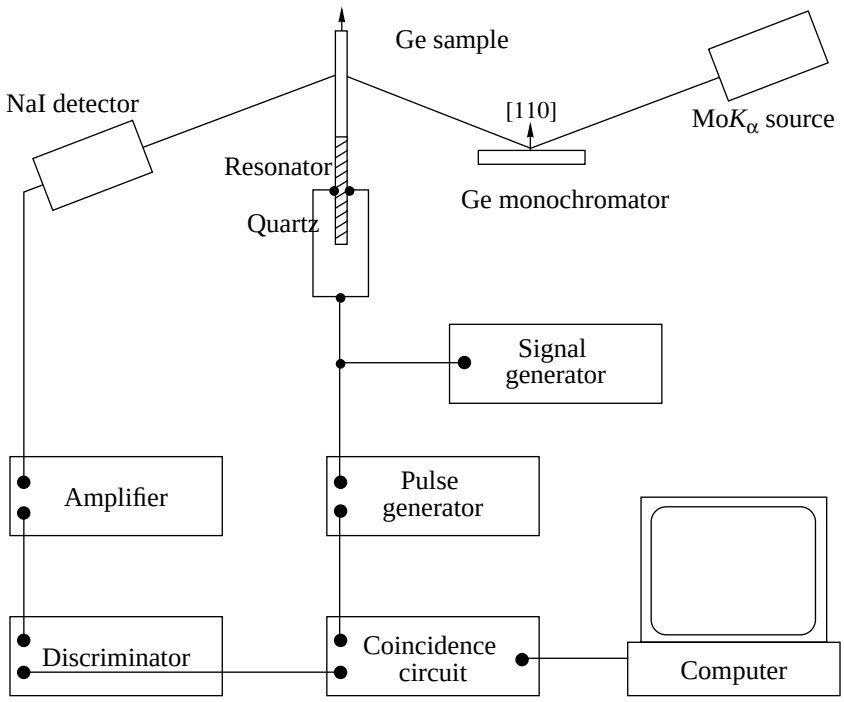

Fig. 4. General experimental scheme for studying the effect of an ultrasonic wave on X-ray diffraction in the crystal.

quality: the DRC half-width is close to the theoretical value and does not exceed 6″ along the whole plate (the angle measurement error was less than half a percent, and the intensity measurement error was less than one percent). The only exception is a region about 3 mm wide next to the place of gluing with the piezoelectric transducer, since it excites ultrasonic deformation. In this region, the DRC differs from a Gaussian shape and has a strongly broadened asymmetric shape caused by a nonuniform static mechanical deformation in the germanium crystal. When ultrasound is turned on, the DRC width increases and the integrated intensity remains the same. The DRC is found to change significantly depending on the X-ray beam position on the crystal. We measured the dependence of the DRC half-width on the X-ray beam coordinate on the sample (Fig. 5). As follows from Fig. 5, short-wave modulation is superimposed on the pure deformation mode, when the half-wavelength of excited ultrasound is along the sample length. This finding indicates the excitation of additional parasitic vibrations and allows us to make preliminary conclusions regarding a real deformation distribution in the sample.

As follows from Fig. 5, the wavelength of the parasitic harmonic is 2.5 mm. This distance is much larger than the X-ray beam width on the crystal (0.2 mm). Note that this modulation substantially increases the deformation gradient in some areas of the crystal across the X-ray beam width. On the other hand, using this modulation, we can create a situation where the acoustic deformation compensates for the static deformation and where the total deformation becomes virtually uniform in a certain portion of the sample.

When ultrasound is turned on, the DRCs in regions close to deformation maxima are strongly broadened (by almost an order of magnitude at the ultrasound amplitudes used) (Fig. 6). In regions with a strong linear ultrasound-deformation gradient, the DRC shape is asymmetric.

We detected a rather interesting effect in a statically stressed region (near the place of gluing with the piezo-

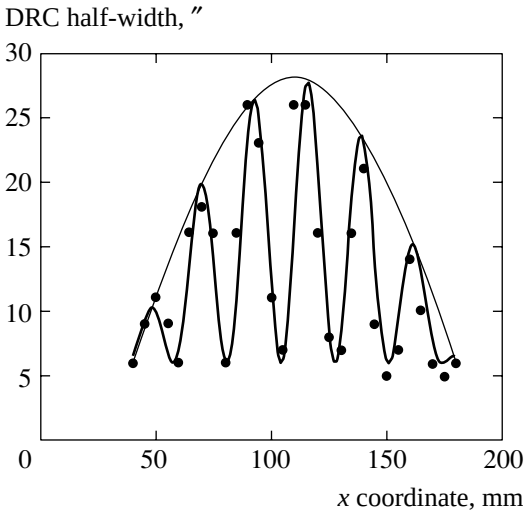

Fig. 5. Dependence of the DRC half-width on the position of an illuminated site on the crystal and the assumed deformation distribution in the case of a pure deformation mode.

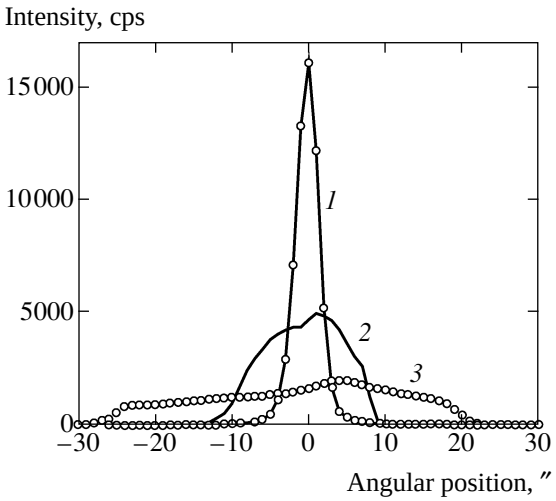

Fig. 6. DRC for Ge(220) at different ultrasound powers. The ultrasound intensity is indicated in percent of the maximum power: (*1*) without ultrasound, (*2*) 40% power, and (*3*) 100% power.

electric transducer). In this region, the DRC has a triangular shape with a large half-width when ultrasound is turned off. If ultrasound is turned on, the rocking curve changes its shape from an asymmetric triangular with a half-width of 50″ to an almost Gaussian shape with a half-width of 15″ (Fig. 7).

3.2. Stroboscopic Measurements

We performed time-resolved (stroboscopic) measurements in several crystal regions with characteristic deformation distributions. First, this is a central region with a quasi-uniform deformation distribution across the beam aperture (region 1). Two other chosen regions have a gradient deformation distribution. One of them is near the free end (region 2), where the DRC half-width without ultrasound is close to the theoretical half-width. The other region (region 3) is chosen near the place of gluing to study the effect of interaction between static and dynamic deformations. In each region, we measured a series of DRC as a function of the resonator vibration phase. The equipment used allowed us to perform stroboscopic measurements with a given delay.

Region 1. The DRCs measured when an X-ray beam passes through the center of the germanium plate at various resonator vibration phases are slightly broadened (Fig. 8). The DRCs measured at phases $\varphi = -\pi/2$ and $\pi/2$ are shifted –20″ and +20″ with respect to the DRC recorded at $\varphi = 0$. These shifts can explain the broadening of the DRC recorded without stroboscopy.

In the germanium crystal, the Bragg condition (more specifically, the Bragg angle) changes because of a periodic change in the lattice parameter, and the center of DRC shifts with respect to the normal (zero) position. In this case, the maximum shift at the center of DRC is 40″; the corresponding change in the lattice parameter is 0.0023 Å; and the relative change is 0.11%.

Region 2. We also carried out measurements at three characteristic values of the vibration phase in the region near the free end of the crystal, where a linear deformation gradient is assumed to occur. The results are shown in Fig. 9. The DRC corresponding to a zero vibration phase is the slightly broadened DRC of the germanium crystal in the absence of ultrasound vibrations. The curves corresponding to vibration phases $\varphi = -\pi/2$ and $\pi/2$ were recorded at the instant of the maximum deformation. They have a complex asymmetric shape that is close to a distorted asymmetric triangle.

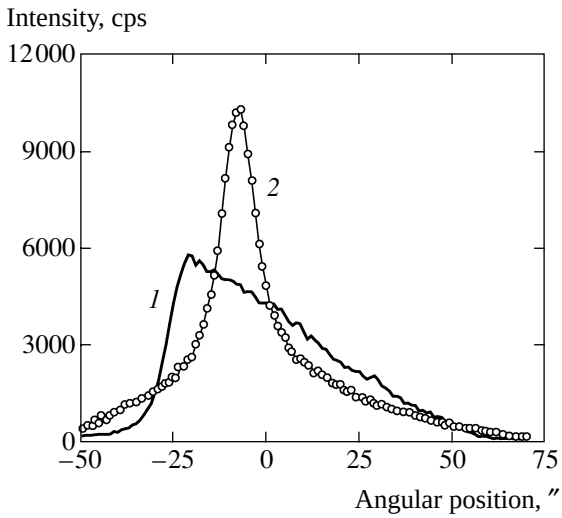

Fig. 7. Effect of ultrasound on the DRC shape of the Ge crystal at the place of gluing with the crystal resonator: (*1*) without and (*2*) with ultrasound.

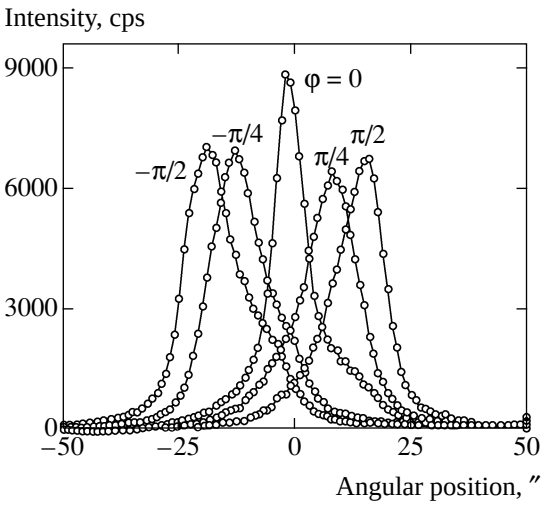

Fig. 8. DRCs measured at different resonator vibration phases. Points stand for experimental data.

The DRC half-width is several times that of the ideal germanium crystal. An analysis of the DRC suggests that, within the X-ray beam width, the deformation is nonuniform and the gradient changes its sign as the sign of the generator vibration phase changes.

Region 3. Figure 10 shows DRCs for the same vibration phases but in the region near the boundary with the piezoelectric element, where the DRC of the unexcited crystal was strongly and asymmetrically broadened because of gluing-induced stresses. In this region, as in the previous case, the ultrasound-induced deformation gradient is almost linear. The curve measured at $\varphi = 0$, as in the previous cases, agrees well with the curve measured without stroboscopy. It has a double-humped shape with a small dip at its center and maxima spaced approximately 100″ apart. The DRC measured at $\varphi = -\pi/2$ has a similar shape, but the intermaximum distance increases approximately to 140″. The amplitude of the higher maximum decreases, and the amplitude of the lower maximum increases by a factor of 1.5. The most interesting effect is observed at a vibration phase $\varphi = \pi/2$, where the amplitude of the higher maximum increases by about an order of magnitude, and the lower maximum almost disappears. The intermaximum distance decreases to 60″. An analysis of these curves suggests that, at different signs of deformation gradients, the ultrasound-induced dynamic deformation partly compensates for the static deformation and that the dynamic deformation enhances the static deformation if their signs coincide.

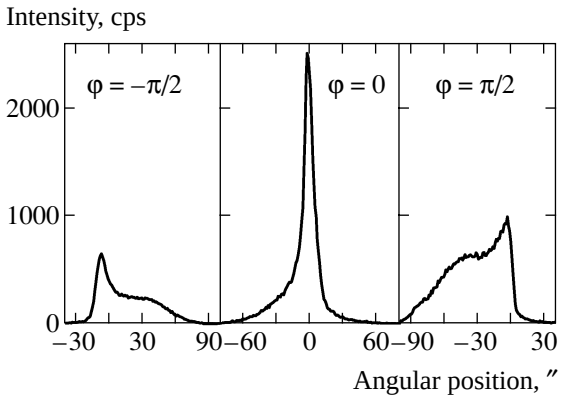

Fig. 9. DRC measured for Ge in the Laue geometry at three characteristic vibration phases in the crystal region where the ultrasound-induced deformation gradient is almost linear.

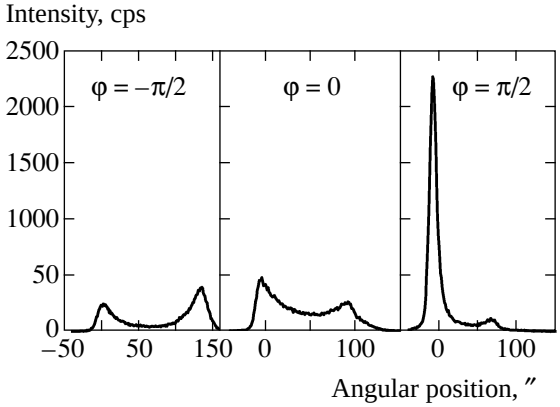

Fig. 10. DRC measured for Ge at three characteristic vibration phases in the statically stressed crystal region. The DRC at $\pi/2$ is shown on a compressed scale.

4. THEORY

In our experiment, the deformation of the crystal substantially breaks the space uniformity in the direction normal to the X-ray beam propagation direction; therefore, the plane wave method, which is usually applied to calculate the angular dependences of the X-ray intensity in the case of diffraction in ideal crystals, is invalid in this case. It should be replaced by the general scheme developed for the calculation of X-ray topograms or phase-contrast images (see [11, 12]). In this scheme, a coherent radiation component is separated in the first stage; it is the monochromatic component of the spherical wave emitted by individual atoms in the anode of an X-ray tube or by orbital electrons in the case of synchrotron radiation. The propagation of this wave along a preferred trajectory (optical axis) is described by Kirchhoff's equations in space and by the Takagi equations in crystals. At the detector, the electric field (amplitude) of this wave and the local intensity (the amplitude modulus squared) depend on the coordinates, and this dependence can be measured with a photographic film or a position-sensitive detector. If the detector counts all photons, the recorded dimensionless intensity (the number of photons per measurement time) is an integral of many parameters with respect to the coherent intensity. The differential intensity should be integrated with respect to all wavelengths, to the source size with allowance for the transverse position of each atom, and to the detector window size. Moreover, we can use the Huygens–Fresnel principle and introduce a propagator for not only space but also for a crystal to describe the diffraction of a point source by the crystal surface.

We have actualized this calculation scheme, and we will use it in our next works. In this work, deformation in the sample changes very slowly over transverse distances comparable with the region of diffraction scattering of a point source located on the sample surface (the so-called Borrmann delta). Moreover, due to sufficiently strong absorption, the transverse size of the diffraction region becomes even narrower. Therefore, by making allowance for the relatively large sizes of the source and the slit that limits the beam in front of the crystal, we can use the so-called "ray" approximation (not to be confused with geometrical optics used for coherent radiation) to ensure a reasonable accuracy. In this approximation, independent trajectories of a coherent X-ray beam in space are considered for each wavelength and each transverse coordinate (point) in the

source; when this beam enters the crystal, it is diffracted by a local region in the crystal as a plane wave.

The result of diffraction of such a local coherent X-ray beam that meets a crystal monochromator and a sample is a function $R(\Delta\theta(s))$ that describes the diffraction reflection curve. This function is dimensionless and presents the convolution of the reflection curves of the monochromator and sample with allowance for the local misfit of the lattice parameters and the angular positions of these two crystals. It is important that this function is independent of the incident-radiation frequency for a dispersion-free scheme. More specifically, the argument is the difference in the Bragg angles in the sample and monochromator, which depends on the coordinate of the incident beam on the sample, since the Bragg angle depends on the coordinate along the plate surface due to a deformation in the sample. In this approach, all the coherent properties of the radiation enter in this function, and various trajectories of the "rays" that correspond to different source points, different frequencies, and different detector coordinates are assumed to be incoherent.

For simplicity, instead of a coordinate x on the crystal, we use a coordinate s on the slit located in front of the crystal. These coordinates are related by a ray trajectory and are at the opposite ends of the trajectory from the slit to the crystal. Since the slit is usually located normal to the optical axis, we have

$$s = Cx\cos\theta_B,$$

where C is the coefficient that is slightly lower than unity and is equal to the ratio of the source–slit to source–crystal distance along the ray trajectory. Thus, we obtain

$$\Delta\theta(s) = \Delta\theta_0 - (\Delta d(s)/s)\tan\theta_B,$$

where $\Delta\theta_0$ is the angle of rotation of the sample about the monochromator; in other words, this is a parameter changing in experiment. On the other hand, $\Delta d(s)$ is the change in the interplanar spacing in the sample as compared to the monochromator. This parameter depends on the crystal deformation, and it is not known in advance.

We introduce a dimensionless normalized function $B(\delta_E)$ to describe the spectral line of the X-ray source as a function of $\delta_E = \Delta E/E$, where E is the photon energy. For the sake of simplicity, we approximate the slit and source by rectangles of widths S and P, respectively, located normal to the trajectory, and the coordinate on the source is denoted by p. Each trajectory begins at a point p on the source and ends in a point s on the slit. In the middle section, the trajectory changes its direction upon reflection by the monochromator, and the point of reflection by the monochromator depends on the photon frequency. Reflection occurs in a very narrow region, which serves as a basis for the application of the ray approximation. Having passed through the slit, the beam broadens substantially after Laue diffraction in the crystal; however, this is not important for us, since the detector records the integrated intensity. The only important parameter is the trajectory coordinate in the crystal. When considering all possible coordinates for the signal measured experimentally, we obtain the formula

$$I(\Delta\theta_0) = I_0 \int_{-P/2}^{P/2} dp \int_{-S/2}^{S/2} ds \int_{-\infty}^{\infty} d\delta_E B(\delta_E) \times \delta(s - p - L_B\delta_E) R(\Delta\theta(s)). \quad (1)$$

Here, the left-hand side contains the dimensionless integrated intensity (the number of photons); $\delta(x)$ is the delta function; and $L_B = L\tan\theta_B$, where L is the source–sample distance; and I_0 is the differential intensity of the incident radiation per unit transverse source length for the whole spectral line width. Like the delta function, this integrated intensity has the dimension of reciprocal length. Note that, in the absence of deformation, all integrals only give the coefficient of proportionality, and the result is equal to $I_0 PR(\Delta\theta_0)$.

In our case, certain simplification can be made, since the $R(\Delta\theta(s))$ function is independent of both the source coordinate and the photon energy. Due to the presence of the delta function, one integral is easily computed, and the result can be written in the form

$$I(\Delta\theta_0) = I_0 L_B^{-1} \int_{-S/2}^{S/2} ds F(s) R(\Delta\theta(s)),$$
$$F(s) = \int_{-P/2}^{P/2} dp B((s-p)/L_B). \quad (2)$$

Formulas (1) and (2) have common features, and the result depends substantially on the source and slit sizes through the $F(s)$ weight function.

In our case, $P/2 = S/2 = 100$ μm and $L_B = 63.5 \times 0.18$ cm = 11.4 cm. Thus, for the center of the slit ($s = 0$), the maximum argument of the function under the integral taken over the source coordinates is equal to 10^{-3}. This value should be compared with the half-width of the Mo$K_{\alpha 1}$ spectral line used in the experiment, which is equal to 3×10^{-4} [13]. It is obvious that, at these parameters, the $F(s)$ function is equal to the integrated value of the spectral function virtually throughout the whole slit width, and it only halves at the slit edges. To a first approximation, we may neglect its shape and change it into unity; then, we have

$$I(\Delta\theta_0) = I_0 \int_{-S/2}^{S/2} ds R(\Delta\theta(s)). \quad (3)$$

With this formula, we can rather simply interpret the experimental curves. The reflection intensity upon diffraction is independent of both the radiation wave-

length and the position of a point source, and it is only specified by the local difference in the Bragg angles in the crystal and monochromator. The summation of the local reflection coefficients does not depend on the trajectory of a certain ray, and it is only determined by the total illumination of each point inside the slit (and, hence, on the crystal surface). This illumination is virtually uniform inside the space limited by the slit. If the deformation is uniform inside the beam width, the experimental curve should be equal to the curve of the ideal crystal, and the peak position can shift if the deformation is nonzero. This experimental result seems to be obvious. If the deformation is nonuniform inside the beam width, we have to integrate the reflection intensity with respect to the beam width by making allowance for the local difference in the Bragg angles at each point.

The experiment shows that some curves have a width well above the width of the reflection curve of the undeformed crystal. In terms of the theoretical model proposed, this means that the deformation in the sample changes sufficiently strongly inside the beam width, so that the region of a changed Bragg angle is significantly larger than the width of the $R(d\theta)$ function. When analyzing such curves, we may neglect the width of the $R(\Delta\theta)$ function and replace it by the $R_0\delta(\Delta\theta)$ function, where R_0 is the integral of the reflection curve of the undeformed crystal. From a physical standpoint, this means that only a part of the beam width having the corresponding Bragg angles is reflected rather than the whole beam width being reflected. The real intensity for every angle of crystal rotation is determined by the width of this part. Assuming that the deformation gradient inside the beam width does not change its sign and using this approximation, we obtain the simple formulas

$$t = (\Delta d/d)\tan\theta_B = \Delta\theta_0, \quad ds/dt = CI(t), \qquad (4)$$

where C is a normalizing constant to be easily determined from the sizes of the angular and spatial regions.

The t parameter specifies the local deformation, and the $t(s)$ function describes the desired deformation profile within the beam width. In real practice, we first determine

$$s(t) = -S/2 + C\int_{t_0}^{t} dxI(x),$$
$$C = S\left(\int_{t_0}^{t_1} dxI(x)\right)^{-1}, \qquad (5)$$

where t_0 and t_1 are the boundaries of the angular region with a noticeable intensity between two pronounced slopes. The desired $t(s)$ function can readily be determined graphically. It directly demonstrates an interplanar-spacing profile in the beam width.

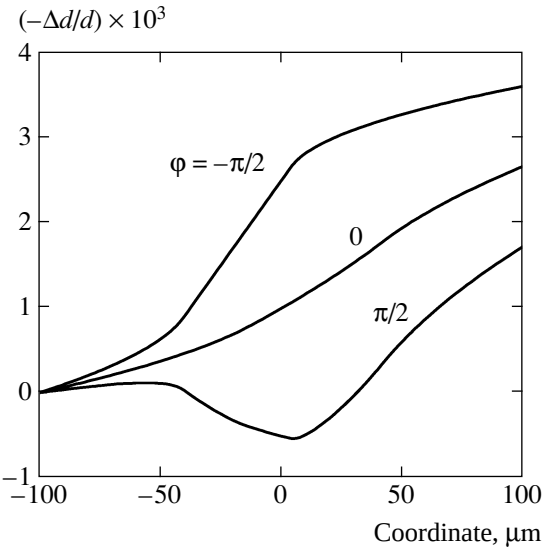

Fig. 11. Deformation profiles calculated from the experimental data for the region near the place of gluing with the resonator (see Fig. 10).

This simple model is found to reliably reconstruct a deformation profile within the beam width from an experimental curve. The experimental curves obtained in region 3 satisfy the conditions of its applicability best of all. Figure 11 shows three curves demonstrating such deformation profiles. The deformation was determined from the angular position of the crystal, and the zero mark was set at the same accuracy. The argument is the position of a point in the illuminated area. The upper curve was calculated by Eqs. (4) and (5) from the experimental curve for a phase $\varphi = -\pi/2$, and the middle curve, from the curve for a phase $\varphi = 0$. It is obvious that, in the second case, the crystal has only a static deformation, whereas, in the first case, an ultrasonic deformation is superimposed on the static deformation. Both deformations have the same sign, which increases the lattice deformation.

Note that the purely ultrasonic deformation can be obtained by the subtraction of the lower curve from the upper curve. For a phase $\varphi = \pi/2$, the result obtained should be subtracted from the purely static deformation. The lower curve in Fig. 11 is obtained as a result of this subtraction. It is seen to have an almost flat long segment in the region of zero deformation. Therefore, this region should correspond to a sharp reflection peak with a width close to the width of the reflection curve of the undeformed crystal. This behavior was detected in the experiment (see Fig. 10). Thus, the compensation of static and dynamic deformations can be described in terms of the model proposed despite the fact that the assumption of a weakly changing deformation within a dynamic diffraction region lies on the boundary of applicability.

The theoretical analysis supports the assumption that, apart from the fundamental long-wave harmonic,

a parasitic harmonic with a smaller spatial period is excited in the crystal.

5. CONCLUSIONS

We were the first to experimentally show the possibility of both uniform and gradient periodic time modulation of the lattice parameter by long-wave ultrasound. This possibility allowed us to electronically control the angular position and the spatial structure of an X-ray beam. When ultrasound is excited in a composite resonator with a thin sample to be measured, we detected a parasitic deformation with a significantly smaller period. This issue has to be studied in more detail. The static deformation was shown to be compensated for by an ultrasound-induced dynamic deformation in the crystal.

We developed a simple theoretical model for X-ray diffraction by a crystal with a spatially nonuniform deformation that is induced by a long-wave ultrasonic wave along the sample surface. Using this model, we described the experimental curves even in the case where deformation changes relatively rapidly.

ACKNOWLEDGMENTS

We thank O.P. Aleshko-Ozheskiĭ, A.A. Lomov, and E.Kh. Mukhamedzhanov for their assistance in the experimental work and for helpful discussions of the results.

This work was supported by the Russian Foundation for Basic Research, project no. 04-02-0817 ofi-a.

REFERENCES

1. I. R. Éntin, Pis'ma Zh. Éksp. Teor. Fiz. **26**, 392 (1977) [JETP Lett. **26**, 269 (1977)].
2. A. Hauer and S. J. Burns, Appl. Phys. Lett. **27**, 524 (1975).
3. D. V. Roshchupkin, R. Tucoulou, M. Brunel, and V. V. Shchelokov, in *Proceedings of All-Russian Meeting on X-ray Optics* (Nizhni Novgorod, 1999), Vol. 1, p. 83.
4. D. Shilo, E. Lakin, E. Zolotoyabko, *et al.*, Synchrotron Radiat. News **15**, 17 (2002).
5. E. Zolotoyabko and J. P. Quintana, Rev. Sci. Instrum. **75**, 699 (2004).
6. R. Tucoulou, D. V. Roshupkin, O. Mathon, *et al.*, J. Synchrotron Radiat. **5**, 1357 (1998).
7. M. A. Navasardyan, J. Appl. Crystallogr. **34**, 763 (2001).
8. V. L. Nosik and M. V. Kovalchuk, Nucl. Instrum. Methods Phys. Res. A **405**, 480 (1998).
9. V. L. Nosik and M. V. Kovalchuk, Poverkhnost, No. 1, 91 (2000).
10. M. V. Koval'chuk, É. K. Kov'ev, and Z. G. Pinsker, Kristallografiya **20**, 142 (1975) [Sov. Phys. Crystallogr. **20**, 81 (1975)].
11. V. G. Kohn, I. Snigireva, and A. Snigirev, Phys. Status Solidi B **222**, 407 (2000).
12. V. G. Kon, Zh. Éksp. Teor. Fiz. **124**, 224 (2003) [JETP **97**, 204 (2003)].
13. M. A. Blokhin and I. G. Shveĭtser, *X-ray Spectrum Handbook* (Nauka, Moscow, 1982), p. 376 [in Russian].

Translated by K. Shakhlevich

Spell: ok